

1 **Multiscale monsoon variability during the last two**  
2 **climatic cycles revealed by spectral signals in Chinese**  
3 **loess and speleothem records**

4  
5 **Y. Li<sup>1</sup>, N. Su<sup>2,3</sup>, L. Liang<sup>1</sup>, L. Ma<sup>1</sup>, Y. Yan<sup>1</sup>, and Y. Sun<sup>1</sup>**

6 <sup>1</sup>State Key Laboratory of Loess and Quaternary Geology, Institute of Earth  
7 Environment, Chinese Academy of Sciences, Xi'an, Shaanxi 710061, China

8 <sup>2</sup>College of Science, Technology and Engineering, James Cook University, Cairns,  
9 Queensland 4870, Australia

10 <sup>3</sup>School of Mathematics and System Science, Shenyang Normal University, Shenyang,  
11 Liaoning 110034, China

12 Correspondence to: Y. Li ([liying@ieecas.cn](mailto:liying@ieecas.cn)) and Y. Sun ([sunyb@ieecas.cn](mailto:sunyb@ieecas.cn))

13

14 **Abstract**

15 The East Asian Monsoon exhibits a significant variability on timescales ranging from  
16 tectonic to centennial as inferred from loess, speleothem and marine records. However,  
17 the relative contributions and plausible driving forces of the monsoon variability at  
18 different timescales remain controversial. Here, we spectrally explore time series of  
19 loess grain size and speleothem  $\delta^{18}\text{O}$  records and decompose the two proxies into  
20 intrinsic components using Empirical Mode Decomposition method. Spectral results  
21 of these two proxies display clear glacial-and-orbital periodicities corresponding to  
22 ice-volume and orbital cycles, and evident millennial signals which are in pace with  
23 Heinrich rhythm and DO cycles. Six intrinsic components are parsed out from loess  
24 grain size and speleothem  $\delta^{18}\text{O}$  records, respectively, and combined signals are  
25 correlated further with possible driving factors including the ice volume, insolation and  
26 North Atlantic cooling. The relative contributions of six components differ

1 significantly between loess grain size and speleothem  $\delta^{18}\text{O}$  records. Coexistence of  
2 glacial and orbital components in the loess grain size implies that both ice volume and  
3 insolation have distinctive impacts on the winter monsoon variability, in contrast to the  
4 predominant precessional impact on the speleothem  $\delta^{18}\text{O}$  variability. Moreover, the  
5 millennial components are evident with variances of 10 % and 17 % in the loess grain  
6 size and speleothem  $\delta^{18}\text{O}$  records, respectively. A comparison of the millennial-scale  
7 signals of these two proxies reveals that abrupt changes in the winter and summer  
8 monsoons over the last 260 kyr share common features and similar driving forces  
9 linked to high-latitude Northern Hemisphere climate.

10

## 11 **1 Introduction**

12 The East Asian Monsoon (EAM), as a significant part of Asian monsoon circulation,  
13 plays an important role in driving the palaeoenvironmental changes in East Asia ([An,  
14 2000](#)). The EAM fluctuations can be quantified at different time intervals ranging  
15 from thousands of years to intraseasonal periodicities, and the primary driving force  
16 of the monsoon variability on each timescale is not unique ([An et al., 2015](#)).  
17 Multiscale monsoon variability has been inferred from numerous proxies generated  
18 from deep-sea sediments (e.g., [Wang et al., 1999](#); [Wang et al., 2005](#)), eolian deposits  
19 (e.g., [An, 2000](#), [Sun et al., 2012](#)), and speleothem records (e.g., [Wang et al., 2001](#),  
20 [2008](#)), which provide valuable insights into the changing processes and potential  
21 driving forces of the EAM variability. In particular, Chinese loess has been  
22 investigated intensively as a direct and complete preserver of the EAM changes, with  
23 great efforts on deciphering on the EAM variability on both orbital and millennial  
24 scales (e.g., [An et al., 1990](#); [Ding et al., 1994, 2002](#); [Porter and An, 1995](#); [Guo et al.,  
25 1996](#); [Chen et al., 1997](#); [Liu and Ding, 1998](#); [Liu et al., 1999](#); [An, 2000](#); [Chen et al.,  
26 2006](#)).

27 On the orbital timescale, the EAM variation recorded by Chinese loess-paleosol  
28 sequences was characterized by an alternation between the dry-cold winter monsoon  
29 and the wet-warm summer monsoon ([Liu and Ding, 1998](#); [An, 2000](#)). A strong 100

1 kyr periodicity was detected in the Chinese loess particle size record, implying an  
2 important impact of glacial boundary conditions on the EAM evolution (Ding et al.,  
3 1995). Obliquity and precession signals were also clear in loess based proxies (Liu et  
4 al., 1999; Ding et al., 2002; Sun et al., 2006). Apart from these dominant periodicities,  
5 some harmonic periodicities related to orbital parameters were also found in the EAM  
6 records, such as the ~75, ~55, and ~30 kyr spectral peaks (Lu et al., 2003; Sun et al.,  
7 2006; Yang et al., 2011). In contrast, absolute-dated speleothem  $\delta^{18}\text{O}$  records revealed  
8 an evident 23 kyr cycle, implying a dominant role of summer insolation in driving the  
9 summer monsoon variability (Wang et al., 2008; Cheng et al., 2009). Different  
10 variances of obliquity and precession signals in monsoonal proxies suggest that the  
11 responses of the winter and summer monsoons to the orbital forcing were dissimilar  
12 (Shi et al., 2011). The various patterns of orbital-scale monsoon fluctuations between  
13 the loess proxies and speleothem  $\delta^{18}\text{O}$  records likely reflected the sensitivity of  
14 various archives and proxies to the EAM variability (Clemens et al., 2010; Cheng et  
15 al., 2012; Sun et al., 2015; Cai et al., 2015).

16 At the millennial timescale, the rapid monsoon oscillations inferred from Chinese  
17 loess were not only persistent during the last two glacial cycles (Porter and An, 1995;  
18 Guo et al., 1996; An and Porter, 1997; Chen et al., 1997; Ding et al., 1999; Sun et al.,  
19 2010; Yang and Ding, 2014), and were also evident during early glacial extreme  
20 climatic conditions (Lu et al., 1999). The millennial-scale monsoon variability during  
21 the last glacial period was strongly coupled to climate changes recorded in Greenland  
22 ice-core and North Atlantic sediments, indicating a dynamic connection between the  
23 EAM variability and the high-latitude Northern Hemisphere climate (Porter and An,  
24 1995; Guo et al., 1996; Chen et al., 1997; Fang et al., 1999). Recently, a combination  
25 of proxies from Chinese loess, speleothem, and Greenland ice-core with modeling  
26 results indicated that the Atlantic meridional overturning circulation might have  
27 played an important role in driving the rapid monsoon changes in East Asia (Sun et al.,  
28 2012).

29

1 Though previous studies have revealed that past EAM variabilities principally  
2 comprise a mixture of forcing signals from ice volume, solar radiation, and North  
3 Atlantic climate, the relative contributions of glacial, orbital and millennial forcing to  
4 the EAM variability remain unclear. In this study, we conducted a comprehensive  
5 investigation of multiscale EAM variability over the last 260 kyr, by analyzing mean  
6 grain size (MGS) record from a Gulang loess sequence (a proxy indicator of the East  
7 Asian winter monsoon intensity) and speleothem  $\delta^{18}\text{O}$  record of Hulu and Sanbao  
8 caves (a debatable indicator of the summer monsoon intensity). These two  
9 representative time series were decomposed to obtain intrinsic components of the  
10 climatic signals, which were further compared with potential driving factors. Our  
11 objectives are to evaluate the relative contributions of glacial–interglacial to  
12 millennial signals registered in these two widely employed monsoon proxies, and to  
13 emphasize the glacial-interglacial discrepancy and millennial similarity between loess  
14 and speleothem records.

15

## 16 **2 Data and methods**

17 The data for the loess sequence was collected at a section in Gulang, Gansu Province,  
18 China (37.49 N, 102.88 E, 2400 ma.s.l.), which is situated in the northwestern part of  
19 the Chinese Loess Plateau. It is about 10 km to the southwest margin of the Tengger  
20 desert (Fig. 1). In this region, the average annual precipitation and temperature over  
21 the last 20 years are 350 mm and 5.7 °C, respectively. About 70 m loess was  
22 accumulated at Gulang during the last two climate cycles. High sedimentation rate  
23 and weak pedogenesis in this region make the Gulang loess sequence very sensitive to  
24 orbital and millennial monsoon changes (Sun et al., 2012, 2015). The samples used in  
25 this study were collected at 2cm intervals, corresponding to 50–100 yr resolution for  
26 the loess-paleosol sequence. Before the measurements of grain sizes, all samples were  
27 firstly pretreated by removing carbonate and organic matter using 30% HCL and 10%  
28  $\text{H}_2\text{O}_2$ , respectively, and then dispersed under ultrasonification in 10ml 10%  $(\text{NaPO}_3)_6$   
29 solution. A Malvern 2000 laser instrument was employed for determining the grain

1 size distribution which has an analytical error of  $< 2\%$  as revealed by replicate  
2 analyses. The grain size data of the upper 20 m were from a 20-m pit near Gulang  
3 (Sun et al., 2012), and the lower part spanning the last two glacial cycles was from  
4 another 50-m section. Mean grain size data of the composite 70-m section have been  
5 employed for a chronological reconstruction (for a detailed description, see Sun et al.,  
6 2015). The Gulang chronology was evaluated by comparison with a 249-kyr grain  
7 size stack (CHILOMOS) record in the northern Loess Plateau (Yang and Ding, 2014)  
8 (Fig.2); the good matches between these two records imply a high reliability of our  
9 Gulang age construction. Unlike previous studies (Sun et al., 2012, 2015), we  
10 performed spectral and decomposing analysis on the mean grain size time series in  
11 order to decipher multiscale variability and dynamics of the winter monsoon.

12 The absolute-dated speleothem  $\delta^{18}\text{O}$  records from Sanbao/Hulu caves (0-224 kyr,  
13 Wang et al., 2008) and the Sanbao cave (224-260 kyr, Cheng et al., 2009) (Fig. 1)  
14 were selected to infer summer monsoon variability spanning the last two  
15 glacial–interglacial cycles. Compatible with the analysis by Wang et al (2008), we  
16 plot the Hulu  $\delta^{18}\text{O}$  data 1.6‰ more negative than that from the Sanbao cave (Fig. 2).  
17 Interpretation of the Chinese speleothem  $\delta^{18}\text{O}$  records remains debatable as a direct  
18 indicator of summer monsoon intensity since various factors like seasonal changes in  
19 precipitation amount, moisture sources, and circulation patterns would influence the  
20 speleothem  $\delta^{18}\text{O}$  composition (e.g., Yuan et al., 2004; Wang et al., 2001, 2008; Cheng  
21 et al., 2009; Clemens et al., 2010; Dayem et al., 2010; Pausata et al., 2011; Maher and  
22 Thompson, 2012; Caley et al., 2014). Nevertheless, high similarity between millennial  
23 events in Chinese speleothem and Greenland ice core revealed that speleothem  $\delta^{18}\text{O}$  is  
24 a reliable indicator of seasonal monsoon change (Wang et al., 2001; Clemens et al.,  
25 2010). More recently, a model-data comparison suggested that Chinese speleothem  
26  $\delta^{18}\text{O}$  can be regarded as a monsoon proxy to reflect the southerly wind intensity rather  
27 than the precipitation change (Liu et al, 2014). Thus, spectral and decomposed results  
28 of the composite speleothem  $\delta^{18}\text{O}$  record time series were used in this study to  
29 address multiscale variability and dynamics of the summer monsoon.

1 To detect the presence of glacial-to-millennial periodicities, we performed spectral  
2 analysis on the 260 kyr records of Gulang MGS and speleothem  $\delta^{18}\text{O}$  using both of  
3 Multitaper (MTM, implemented in the SSA toolkit, [Vautard et al., 1992](#))  
4 (<http://www.atmos.ucla.edu/tcd/ssa/>) and REDFIT ([Schulz and Mudelsee, 2002](#))  
5 methods, which are related to Empirical Orthogonal Function and Lomb–Scargle  
6 Fourier transform, respectively. MTM method has the advantages of being suitable  
7 for series affected by high-noise levels, and incorporating significance test which is  
8 not proportional to the power of spectrum, confirming the detection of low-amplitude  
9 periodicities ([Lu et al., 1999](#)), while the REDFIT program estimates the first-order  
10 autoregressive (AR1) parameter from unevenly spaced time series without  
11 interpolation, which avoids a too “red” spectrum ([Schulz and Stattgeger, 1997](#)). The  
12 similar spectral periodicities derived from both REDFIT and MTM methods were  
13 regarded as dominant frequencies at glacial-to-millennial bands.

14 The decomposed components of loess MGS and speleothem  $\delta^{18}\text{O}$  records were parsed  
15 out using the technique of Empirical Mode Decomposition (EMD) ([Huang et al.,](#)  
16 [1998](#)). EMD directly extracts energy which is associated with intrinsic time scales in  
17 nonlinear fluctuations, and iteratively decomposes the raw complex signal with  
18 several characteristic time scales coexisting into a series of elementary intrinsic model  
19 function (IMF) components, avoiding any arbitrariness in the choices of frequency  
20 bands in this multiscale study. The EMD method has been widely employed over  
21 various palaeoclimate database, such as ice-cover ([Gloersen and Huang, 2003](#)), North  
22 Atlantic oscillation ([Hu and Wu, 2004](#)), solar insolation ([Lin and Wang, 2006](#)), and  
23 temperature under global warming ([Molla et al., 2006](#)). However, the application of  
24 EMD method on the loess record remains poorly investigated with some  
25 understanding of decomposed components at glacial-and-orbital scale ([Yang et al.,](#)  
26 [2001, 2008](#)). In this study, we applied EMD on high-resolution loess and speleothem  
27 data records to quantify the relative contributions of both orbital and millennial  
28 components.

29

### 1 **3 Multiscale monsoon variability**

2 The highly comparable spectral results between REDFIT and MTM methods show  
3 that apparent periods identified in the MGS spectrum are at ~100, ~41, ~23, ~15, ~7,  
4 ~5, and ~3-1 kyr over the 80 % and 90 % confidence levels, respectively, for REDFIT  
5 and MTM methods (Fig. 3). It is shown that the potential forcing of the  
6 glacial–interglacial and orbital EAM variability is part of the external (e.g., the  
7 orbital-induced summer insolation, [An, 1991](#); [Wang et al., 2008](#)) and the internal  
8 factors (e.g., the changes in the ice volume and CO<sub>2</sub> concentrations, [Ding et al., 1995](#);  
9 [Lu et al., 2013](#); [Sun et al., 2015](#)). The coexistence of the ~100, ~41, and ~23 kyr  
10 periods in the Gulang MGS record confirms the dynamic linkage of the winter  
11 monsoon variability to glacial and orbital forcing. Based on the spectral results, many  
12 millennial frequencies are detected, which can be mainly divided into two groups of  
13 ~7-5 and ~3-1 kyr, which, possibly correspond, respectively, to the Heinrich (~6 kyr)  
14 rhythm and the Dansgaard–Oeschger (DO, ~1.5 kyr) cycles recorded in the North  
15 Atlantic sediments and Greenland ice core ([Bond et al., 1993](#); [Dansgaard et al., 1993](#);  
16 [Heinrich, 1988](#)). Taking into account the sampling resolution and surface mixing  
17 effect at Gulang, the residual component (< 1 kyr) might contain both centennial and  
18 noisy signals, which is excluded for further discussion in this study.

19 Compared to the MGS spectral results, the speleothem  $\delta^{18}\text{O}$  spectrum shares similar  
20 peaks at the precession (~23 kyr) and millennial bands (~5, ~3, ~2.4, ~2, ~1.5, ~1.3,  
21 and ~1 kyr), but is lack of distinct peaks at ~100 kyr and ~41 kyr (Fig. 3). Notably,  
22 precession peaks at ~23 and ~19 kyr are more dominant in the speleothem  $\delta^{18}\text{O}$  than  
23 in the loess MGS record. Moreover, the speleothem spectrum shows a peak over the  
24 80 % and 90 % confidence levels in REDFIT and MTM spectrum, respectively,  
25 centered at ~10 kyr frequency, which is, approximately, related to the semi-precession  
26 frequency.

27 The different oscillation patterns composing loess MGS and speleothem  $\delta^{18}\text{O}$  time  
28 series are separated out using EMD method as presented in Fig. 4 and Fig. 5,  
29 respectively, together with dominant periods as shown. Six IMFs are generated for the

1 Gulang MGS data on glacial-to-millennial timescale. The periodicities in IMF3 span  
2 19-10 kyr likely correspond to the second precessional cycle. The variability of  
3 Gulang MGS is dominated by the lowest frequency signal with variances of 38 %  
4 (IMF6). Two orbital components (IMF5 and IMF4) are linked to obliquity and  
5 precession, contributing equally 23 % to the total variance. The variances of two  
6 millennial components (IMF2 and IMF1) are very close (5 %) in the Gulang MGS  
7 record. Similarly, six IMFs are decomposed for the speleothem  $\delta^{18}\text{O}$  record on  
8 frequencies lower than 1 kyr, and all the glacial-to-orbital periodicities correspond to  
9 Milankovitch parameters. Compared with decomposed results of Gulang MGS record,  
10 glacial (IMF6) and obliquity (IMF5) components are not clear in the speleothem  $\delta^{18}\text{O}$   
11 record with variances of 11 % and 8 %, respectively. The precession component  
12 (IMF4), however, is the most dominant signal among the six components, accounting  
13 for 56 % of the variance. A notable semi-precession component (IMF3) contributes 8 %  
14 of the total variance, and two millennial components are also evident with variances  
15 of 12 % and 5 %, respectively.

16

## 17 **4 Dynamics of multiscale EAM variability**

### 18 **4.1 Glacial and orbital forcing of the EAM variability**

19 We combine IMF3, 4, 5, and 6 of Gulang MGS and speleothem  $\delta^{18}\text{O}$  records as the  
20 low-frequency signals ( $>10$  kyr) to reveal the glacial-and-orbital scale variations of the  
21 winter and summer monsoon, respectively. The glacial-and-orbital variations of the  
22 loess and speleothem records represent the total variances of  $\sim 90$  % and  $\sim 83$  %,   
23 respectively. The low-frequency signals of the loess MGS and speleothem  $\delta^{18}\text{O}$  records  
24 are compared with changes in the ice volume and solar insolation at  $65^\circ\text{N}$  ([Berger, 1978](#)),  
25 to ascertain plausible impacts of glacial and orbital factors on the EAM  
26 variability (Fig. 6).

27 The low-frequency component of the Gulang MGS record is well correlated with  
28 global ice volume change inferred from the benthic  $\delta^{18}\text{O}$  record ([Lisiecki and Raymo,](#)



1 2005), reinforcing the strong coupling between the winter monsoon variation and  
2 ice-volume changes (Ding et al., 1995). Besides the glacial–interglacial contrast, fine  
3 MGS signals at the precessional scale seem more distinctive than those in the benthic  
4  $\delta^{18}\text{O}$  stack. For example, the remarkable peaks in the MGS around 50, 85, 110, and 170  
5 kyr have no counterpoints in the benthic  $\delta^{18}\text{O}$  record. By comparing MGS data with the  
6 summer insolation record, the overall ~20 kyr periodicity is damped but still visible  
7 during both glacial and interglacial periods, except for insolation maxima around 150  
8 and 220 kyr (Fig. 6). The coexistence of the glacial and orbital cycles in loess MGS  
9 indicates that both the ice volume and solar insolation have affected the winter  
10 monsoon variability, and their relative contributions are 38 % and 52 %, respectively,  
11 as estimated from variances of the glacial (IMF6) and orbital (IMF5-3) components.

12 The speleothem  $\delta^{18}\text{O}$  record varies quite synchronously with the July insolation,  
13 characterized by a dominant precession frequency (Fig. 6). This in-phase change is  
14 thought to support a dominant role of summer insolation in the Northern Hemisphere in  
15 driving the summer monsoon variability at the precession period (Wang et al., 2008),  
16 given that the palaeoclimatic interpretation of the speleothem  $\delta^{18}\text{O}$  is quite  
17 controversial (Wang et al., 2001, 2008; Yuan et al., 2004; Hu et al., 2008; Cheng et al.,  
18 2009; Peterse et al., 2011).

19 The different contributions of glacial and orbital variability in the loess MGS and  
20 speleothem  $\delta^{18}\text{O}$  records indicate that the driving forces associated with these two  
21 proxies are different. The loess grain size is directly related to the northwesterly wind  
22 intensity, reflecting that atmospheric surface process is linked to the  
23 Siberian-Mongolian High (Porter and An, 1995). The speleothem  $\delta^{18}\text{O}$  might be  
24 influenced by multiple factors such as the isotopic depletion along the vapor transport  
25 path (Pausata et al., 2011), changes in  $\delta^{18}\text{O}$  values of meteoric precipitation or the  
26 amount of summer monsoon precipitation (Wang et al., 2001, 2008; Cheng et al., 2009),  
27 and seasonality in the amount and isotopic composition of rainfall (Clemens et al., 2010;  
28 Dayem et al., 2010; Maher and Thompson, 2012).

29 It is quite clear that the EAM is formed by the thermal gradient between the Asian

1 continent and the Pacific Ocean to the east and southeast (Halley, 1986; Xiao et al.,  
2 1995; Lestari and Iwasaki, 2006). In winter, due to a much larger heat capacity of water  
3 in the ocean than that on the land surface, a higher barometric pressure forms over the  
4 colder Asian continent with a lower pressure over the warmer ocean. This gradient is  
5 the driving force for the flow of cold and dry air out of Asia, consequently, the winter  
6 monsoon forms (Gao, 1962). On the glacial–interglacial timescale, the buildup of the  
7 northern high-latitude ice sheets during the glacial periods strengthens the barometric  
8 gradient which results in intense winter monsoons (Ding et al., 1995; Clark et al., 1999).  
9 The contemporaneous falling sea level and land-ocean pressure gradient further  
10 enhances winter monsoon circulation during glacial times (Xiao et al., 1995). The  
11 other factor that influences the land-ocean differential thermal motion is the orbitally  
12 induced solar radiation changes. The precession-induced insolation changes can lead to  
13 regional land-ocean thermal gradients whilst obliquity-related insolation changes can  
14 result in meridional thermal gradients; both of which can substantially alter the  
15 evolution of the Siberian and Subtropical Highs and the EAM variations (Shi et al.,  
16 2011).

#### 17 **4.2 Impacts of high-latitude cooling on millennial EAM oscillations**

18 The EAM variations are persistently punctuated by apparent millennial-scale  
19 monsoon events (Garidel-Thoron et al., 2001; Wang et al., 2001; Kelly et al., 2006).  
20 The millennial-scale events of the last glacial cycle were firstly identified in  
21 Greenland ice cores (Dansgaard et al., 1993; Meese et al., 1997). Subsequently,  
22 well-dated loess grain size and speleothem  $\delta^{18}\text{O}$  records in China have been found to  
23 have apparent correspondences with rapid climate oscillations in the North Atlantic  
24 (Porter and An, 1995; Guo et al., 1996; Chen et al., 1997; Ding et al., 1998; Wang et  
25 al., 2001). The most striking evidence is the strong correlation between the loess grain  
26 size, speleothem  $\delta^{18}\text{O}$  and Greenland ice core  $\delta^{18}\text{O}$  records during the last glaciation  
27 (Ding et al., 1998; Wang et al., 2001; Sun et al., 2012). These abrupt changes have  
28 been extended into the past glacial–interglacial cycles from loess and speleothem  
29 records (Ding et al., 1999; Cheng et al., 2006, 2009; Wang et al., 2008; Yang and

1 [Ding, 2014](#)) and from the North Atlantic sediments ([McManus et al., 1999](#); [Channell](#)  
2 [et al., 2012](#)).

3 Here IMF1 and 2 components of the loess MGS and speleothem  $\delta^{18}\text{O}$  records are  
4 combined to be considered as millennial-scale signals of the winter and summer  
5 monsoons, with variances of 10 % and 17 %, respectively. The combination of the  
6 two millennial signals of the loess MGS and speleothem  $\delta^{18}\text{O}$  records are compared  
7 with the North Atlantic cooling events over the last two glacial cycles, to reveal the  
8 dynamic links of abrupt climate changes in East Asia and the North Atlantic (Fig. 7).  
9 The Younger Dryas (YD) and Heinrich Events (H<sub>1</sub>-H<sub>6</sub>) are well detected in loess and  
10 speleothem records around 12, 16, 24, 31, 39, 48, 55, and 60 kyr, respectively. Most  
11 of the millennial-scale events in the loess MGS and speleothem  $\delta^{18}\text{O}$  records are well  
12 aligned with comparable amplitude and duration during the last two glacial cycles.  
13 However, some MGS valleys such as A17, A23, and B17-19 are not well matched  
14 with the speleothem  $\delta^{18}\text{O}$  minima, possibly due to uncertainties in the loess  
15 chronology. The comparable millennial scale events between grain size of Gulang and  
16 CHILOMOS stack ([Yang and Ding, 2014](#)) shows the nature of replication of Gulang  
17 MGS record within the dating uncertainty, confirming the persistent millennial-scale  
18 winter monsoon variability spanning the last two glacial cycles (Fig. 7).

19 The millennial-scale monsoon signals have been well compared with the cooling  
20 events recorded in the North Atlantic sediments, demonstrating a dynamic link  
21 between abrupt climate changes in East Asia and the North Atlantic. As identified in  
22 Chinese speleothem records, the magnitudes of abrupt climate events are identical  
23 between the last and the penultimate climatic cycles ([Wang et al., 2008](#)). However,  
24 the duration and amplitude of these millennial events seems quite different between  
25 the glacial and interglacials. The duration of millennial monsoon events is relatively  
26 shorter and the amplitude larger during glacial periods, suggesting a plausible glacial  
27 modulation on rapid climate changes ([McManus et al., 1999](#); [Wang et al., 2008](#)). The  
28 potential driving mechanism for rapid EAM changes has been attributed to changing  
29 climate in the high-latitude Northern Hemisphere, e.g., the reduction of the North

1 Atlantic deep water circulation triggered by fresh water inputs from melting icebergs  
2 (Broecker, 1994). The North Atlantic cooling can affect the zonal high pressure  
3 systems, including the Azores- Ural-Siberian-Mongolian high (Palmer and Sun, 1985;  
4 Rodwell et al., 1999; Yuan et al., 2004), which can further transmit the abrupt cooling  
5 effect into East Asia and result in significant EAM changes (Porter and An, 1995;  
6 Wang et al., 2001). Apart from the geological evidence, numerical modeling also  
7 suggests that the Atlantic meridional overturning circulation might affect abrupt  
8 oscillations of the EAM, while the westerly jet is the important conveyor introducing  
9 the North Atlantic signal into the EAM region (Miao et al., 2004; Zhang and  
10 Delworth, 2005; Jin et al., 2007; Sun et al., 2012).

11

## 12 **5 Conclusions**

13 The multiscale signals were spectrally detected and naturally decomposed from  
14 Chinese loess and speleothem records over the last two climatic cycles, permitting an  
15 evaluation of the relative contributions of glacial, orbital and millennial components in  
16 the EAM record. Spectrum of Gulang MGS and speleothem  $\delta^{18}\text{O}$  data show similar  
17 periodicities at glacial-to-orbital and millennial timescales, corresponding to the  
18 rhythms of changing ice-volume, orbitally induced insolation, and North Atlantic  
19 cooling (i.e., Heinrich rhythm and Dansgaard–Oeschger cycles), respectively.  
20 Amplitude variances of the decomposed components reveal significant glacial and  
21 orbital impacts on the loess grain size variation and a dominant precession forcing in  
22 the speleothem  $\delta^{18}\text{O}$  variability. The millennial components are evident in the loess and  
23 speleothem proxies with variances of 10 % and 17 %, respectively. Two millennial  
24 IMFs were combined to recognize the synchronous nature of rapid changes of these  
25 two proxies. High similarity of millennial-scale monsoon events both in terms of the  
26 magnitudes and rhythms between the loess and speleothem proxies implies that the  
27 winter and summer monsoons share common millennial features and similar driving  
28 forces.

29

1 **Acknowledgements**

2 We thank J. Zhao, L. He, M. Zhao, and H. Wang for assistance in field sampling and lab  
3 measurements. Three anonymous reviewers and Dr. Loutre Marie-France are  
4 acknowledged for their insightful comments. This work was supported by funds from  
5 the National Basic Research Program of China (2013CB955904), the Chinese  
6 Academy of Sciences (KZZD-EW25 TZ-03), the National Science Foundation of  
7 China (41472163), and the State Key Laboratory of Loess and Quaternary Geology  
8 (SKLLQG1011).

1 **References**

2 An, Z. and Porter, S. C.: Millennial-scale climatic oscillations during the last  
3 interglaciation in central China, *Geology*, 25, 603–606, 1997.

4 An, Z., Liu, T., Lu, Y., Porter, S. C., Kukla, G., Wu, X., and Hua, Y.: The long-term  
5 paleomonsoon variation recorded by the loess-paleosol sequence in Central China,  
6 *Quatern. Int.*, 7, 91–95, 1990.

7 An, Z., Wu, G., Li, J., Sun, Y., Liu, Y., Zhou, W., Cai, Y., Duan, A., Li, L., Mao, J.,  
8 Cheng, H., Shi, Z., Tan, L., Yan, H., Ao, H., Chang, H., and Juan, F.: Global  
9 monsoon dynamics and climate change, *Annu. Rev. Earth. Planet. Sci.*, 42,  
10 doi:10.1146/annurev-earth-060313-054623, 2015.

11 An, Z.: Magnetic susceptibility evidence of monsoon variation on the Loess Plateau  
12 of central China during the last 130,000 years, *Quaternary Res.*, 36, 29–36, 1991.

13 An, Z.: The history and variability of the East Asian paleomonsoon climate,  
14 *Quaternary Sci. Rev.*, 19, 171–187, 2000.

15 Berger, A.: Long-term variations of daily insolation and Quaternary climate changes,  
16 *J. Atmos. Sci.*, 35, 2362-2367, 1978.

17 Bond, G., Broecker, W., Johnsen, S., McManus, J., Labeyrie, L., Jouzel, J., and  
18 Bonani, G.: Correlations between climate records from North Atlantic sediments and  
19 Greenland ice, *Nature*, 365, 143–147, 1993.

20 Broecker, W. S.: Massive iceberg discharges as triggers for global climate change,  
21 *Nature*, 372, 421–424, 1994.

22 Cai, Y., Fung, I. Y., Edwards, R. L., An, Z., Cheng, H., Lee, J. E., Tan, L., Shen, C.  
23 C., Wang, X., Day, J. A., Zhou, W. J., Kelly, M. J., and Chiang, J. C. H.: Variability  
24 of stalagmite-inferred Indian monsoon precipitation over the past 252,000 y, *Proc.*  
25 *Natl. Acad. Sci. U. S. A.*, 112, 2954-2959, 2015.

26 Caley, T., Roche, D. M., and Renssen, H.: Orbital Asian summer monsoon dynamics  
27 revealed using an isotope-enabled global climate mode, *Nat. Commun.*, 5,

1 doi:10.1038/ncomms6371, 2014.

2 Channell, J. E. T., Hodell, D. A., Romero, O., hillaire-Marcel, C., Vernal, A. D.,  
3 Stoner, J. S., Mazaud, A., and Röhl, U.: A 750-kyr detrital-layer stratigraphy for the  
4 North Atlantic (IODP Sites U1302–U1303, Orphan Knoll, Labrador Sea), *Earth*  
5 *Planet. Sc. Lett.*, 317–318, 218–230, 2012.

6 Chen, F., Bloemendal, J., Wang, J., Li, J., and Oldfield, F.: High-resolution  
7 multi-proxy climate records from Chinese loess: evidence for rapid climatic changes  
8 over the last 75 kyr, *Palaeogeogr. Palaeoclimatol.*, 130, 323–335, 1997.

9 Chen, J., Chen, Y., Liu, L., Ji, J., Balsam, W., Sun, Y., and Lu, H.: Zr/Rb ratio in the  
10 Chinese loess sequences and its implication for changes in the East Asian winter  
11 monsoon strength, *Geochim. Cosmochim. Acta.*, 70, 1471–1482, 2006.

12 Cheng, H., Edwards, R. L., Broecker, W. S., Denton, G. H., Kong, X., Wang, Y.,  
13 Zhang, R., and Wang, X.: Ice age terminations, *Science*, 326, 248–252, 2009.

14 Cheng, H., Edwards, R. L., Kong, X., Ming, Y., Kelly, M. J., Wang, X., Gallup, C. D.,  
15 and Liu, W.: A penultimate glacial monsoon record from Hulu Cave and two-phase  
16 glacial terminations, *Geology*, 34, 217–220, 2006.

17 Cheng, H., Zhang, P., Spötl, C., Edwards, R. L., Cai, Y., Zhang, D., and Sang, W.:  
18 The climate cyclicality in semiarid-arid central Asia over the past 500,000 years,  
19 *Geophys. Res. Lett.*, 39, L01705, doi:10.1029/2011GL050202, 2012.

20 Clark, P. U., Alley, R. B., and Pollard, D.: Northern Hemisphere ice-sheet influences  
21 on global climate change, *Science*, 286, 1104–1111, 1999.

22 Clemens, S. C., Prell, W. L., and Sun, Y.: Orbital-scale timing and mechanisms  
23 driving Late Pleistocene Indo-Asian summer monsoons: reinterpreting cave  
24 speleothem  $\delta^{18}\text{O}$ , *Paleoceanography*, PA4207, doi:10.1029/2010PA001926, 2010.

25 Dansgaard, W., Johnsen, S. J., Clausen, H. B., Dahl-Jensen, D., Gundestrup, N. S.,  
26 Hammer, C. U., Hvidberg, C. S., Steensen, J. P., Sveinbjornsdottir, A. E., Jouzel, J.,  
27 and Bond, G.: Evidence for general instability of past climate from a 250-kyr ice-core

1 record, *Nature*, 364, 218–220, 1993.

2 Dayem, K. E., Molnar, P., Battisti, D. S., and Roe, G. H.: Lessons learned from  
3 oxygen isotopes in modern precipitation applied to interpretation of speleothem  
4 records of paleoclimate from eastern Asia, *Earth Planet. Sc. Lett.*, 295, 219–230,  
5 2010.

6 Ding, Z., Derbyshire, E., Yang, S., Yu, Z., Xiong, S., and Liu, T.: Stacked 2.6-Ma  
7 grain size record from the Chinese loess based on five sections and correlation with  
8 the deep-sea  $\delta^{18}\text{O}$  record, *Paleoceanography*, 17, 5-1-5-21, 2002.

9 Ding, Z., Liu, T., Rutter, N. W., Yu, Z., Guo, Z., and Zhu, R.: Ice-Volume forcing of  
10 East Asian winter monsoon variations in the past 800,000 years, *Quaternary Res.*, 44,  
11 149–159, 1995.

12 Ding, Z., Ren, J., Yang, S., and Liu, T.: Climate instability during the penultimate  
13 glaciation: evidence from two high-resolution loess records, China, *J. Geophys. Res.*,  
14 104, 20123–20132, 1999.

15 Ding, Z., Rutter, N. W., Liu, T., Ren, J., Sun, J., and Xiong, S.: Correlation of  
16 Dansgaard–Oeschger cycles between Greenland ice and Chinese loess, *Paleoclimates*,  
17 4, 281–291, 1998.

18 Ding, Z., Yu, Z., Rutter, N. W., and Liu, T.: Towards an orbital time scale for Chinese  
19 loess deposits, *Quaternary Sci. Rev.*, 13, 39–70, 1994.

20 Fang, X., Pan, B., Guan, D., Li, J., Yugo, O., Hitoshi, F., and Keiichi, O.: A  
21 60000-year loess-paleosol record of millennial-scale summer monsoon instability  
22 from Lanzhou, China, *Chinese Sci. Bull.*, 44, 2264–2267, 1999.

23 Gao, Y.: On some problems of Asian monsoon, in: *Some Questions About the East*  
24 *Asian Monsoon*, edited by: Gao, Y., Science Press, Beijing, 1–49, 1962.

25 Garidel-Thoron, T. D., Beaufort, L., Linsley, B. K., and Dannenmann, S.:  
26 Millennial-scale dynamics of the East Asian winter monsoon during the last 200,000  
27 years, *Paleoceanography*, 16, 491–502, 2001.



1 Gloersen, P. and Huang, N.: Comparison of interannual intrinsic modes in  
2 hemispheric ice covers and other geophysical parameters, *IEEE Transactions in*  
3 *Geosciences and Remote Sensing*, 41, 1062-1074, 2003.

4 Guo, Z., Liu, T., Guiot, J., Wu, N., Lv, H., Han, J., Liu, J., and Gu, Z.: High  
5 frequency pulses of East Asian monsoon climate in the last two glaciations: link with  
6 the North Atlantic, *Clim. Dynam.*, 12, 701–709, 1996.

7 Halley, E.: An historical account of the trade winds and monsoons observable in the  
8 seas between and near the tropics with an attempt to assign the physical cause of the  
9 said wind, *Philos. T. R. Soc. Lond.*, 16, 153–168, 1986.

10 Heinrich, H.: Origin and consequences of cyclic ice rafting in the Northeast Atlantic  
11 Ocean during the past 130,000 years, *Quaternary Res.*, 29, 142–152, 1988.

12 Hu, C., Henderson, G. M., Huang, J., Xie, S., Sun, Y., and Johnson, K. R.:  
13 Quantification of Holocene Asian monsoon rainfall from spatially separated cave  
14 records, *Earth Planet. Sc. Lett.*, 266, 221–232, 2008.

15 Hu, Z. and Wu, Z.: The intensification and shift of the annual North Atlantic  
16 Oscillation in a global warming scenario simulation, *Tellus*, 56, 112-124, 2004.

17 Huang, N. E., Shen, Z., Long, S. R., Wu, M. C., Shih, H. H., Zheng, Q., Yen, N. C.,  
18 Tung, C. C., and Liu, H. H.: The empirical mode decomposition and the Hilbert  
19 spectrum for nonlinear and non-stationary time series analysis, *The Royal Society*,  
20 454, 903-995, 1998.

21 Jin, L., Chen, F., Ganopolski, A., and Claussen, M.: Response of East Asian climate  
22 to Dansgaard/Oeschger and Heinrich events in a coupled model of intermediate  
23 complexity, *J. Geophys. Res.*, 112, D06117, doi:10.1029/2006JD007316, 2007.

24 Kelly, M. J., Edwards, R. L., Cheng, H., Yuan, D., Cai, Y., Zhang, M., Lin, Y., and  
25 An, Z.: High resolution characterization of the Asian Monsoon between 146,000 and  
26 99,000 years B. P. from Dongge Cave and global correlation of events surrounding  
27 Termination II, *Palaeogeogr. Palaeoclimatol.*, 236, 20–38, 2006.

1 Lestari, R. and Iwasaki, T.: A GCM study on the roles of the seasonal marches of the  
2 SST and land–sea thermal contrast in the onset of the Asian summer monsoon, *J.*  
3 *Meteorol. Soc. Jpn.*, 84, 69–83, 2006.

4 Lin, Z. and Wang, S.: EMD analysis of solar insolation, *Meteorol. Atoms. Phys.*, 93,  
5 123-128, 2006.

6 Lisiecki, L. E. and Raymo, M. E.: A Pliocene-Pleistocene stack of 57 globally  
7 distributed benthic  $\delta^{18}\text{O}$  records, *Paleoceanography*, 20, PA1003,  
8 doi:10.1029/2004PA001071, 2005.

9 Liu, T. and Ding, Z.: Chinese loess and the paleomonsoon, *Annu. Rev. Earth Pl. Sc.*,  
10 26, 111– 145, 1998.

11 Liu, T., Ding, Z., and Rutter, N.: Comparison of Milankovitch periods between  
12 continental loess and deep sea records over the last 2.5 Ma, *Quaternary Sci. Rev.*, 18,  
13 1205–1212, 1999.

14 Liu, Z., Wen, X., Brady, E. C., Otto-Bliesner, B., Yu, G., Lu, H., Cheng, H., Wang,  
15 Y., Zheng, W., Ding, Y., Edwards, R. L., Cheng, J., Liu, W., and Yang, H.: Chinese  
16 cave records and the East Asian Summer Monsoon, *Quaternary Sci. Rev.*, 83,  
17 115-128, 2014.

18 Lu, H., Huissteden, K. V., An, Z., Nugteren, G., and Vandenberghe, J.: East Asia  
19 winter monsoon variations on a millennial time-scale before the last  
20 glacial–interglacial cycle, *J. Quaternary Sci.*, 14, 101–110, 1999.

21 Lu, H., Yi, S., Liu, Z., Mason, J. A., Jiang, D., Cheng, J., Stevens, T., Xu, Z., Zhang,  
22 E., Jin, L., Zhang, Z., Guo, Z., Wang, Y., and Otto-Bliesner, B.: Variation of East  
23 Asian monsoon precipitation during the past 21 k.y., and potential CO<sub>2</sub> forcing,  
24 *Geology*, 41, 1023–1026, 2013.

25 Lu, H., Zhang, F., and Liu, X.: Patterns and frequencies of the East Asian winter  
26 monsoon variations during the past million years revealed by wavelet and spectral  
27 analyses, *Global Planet. Change*, 35, 67–74, 2003.

1 Maher, B. A. and Thompson, R.: Oxygen isotopes from Chinese caves: records not of  
2 monsoon rainfall but of circulation regime, *J. Quaternary Sci.*, 27, 615–624, 2012.

3 McManus, J. F., Oppo, D. W., and Cullen, J. L.: A 0.5-million-year record of  
4 millennial-scale climate variability in the North Atlantic, *Science*, 283, 971–975,  
5 1999.

6 Meese, D. A., Gow, A. J., Alley, R. B., Zielinski, G. A., Grootes, P. M., Ram, M.,  
7 Taylor, K. C., Mayewski, P. A., and Blozan, J. F.: The Greenland Ice Sheet Project 2  
8 depth-age scale: methods and results, *J. Geophys. Res.*, 102, 26411–26423, 1997.

9 Miao, X., Sun, Y., Lu, H., and Mason, J. A.: Spatial pattern of grain size in the Late  
10 Pliocene “Red Clay” deposits (North China) indicates transport by low-level northerly  
11 winds, *Palaeogeogr. Palaeoclimatol.*, 206, 149–155, 2004.

12 Molla, K., Sumi, A., and Rahman, M.: Analysis of temperature change under global  
13 warming impact using Empirical Mode Decomposition, *Int. J. Information Technol.*,  
14 3, 131-139, 2006.

15 Palmer, T. N. and Sun, Z.: A modelling and observational study of the relationship  
16 between sea surface temperature in the North-West Atlantic and the atmospheric  
17 general circulation, *Q. J. Roy. Meteor. Soc.*, 111, 947–975, 1985.

18 Pausata, F. S. R., Battisti, D. S., Nisancioglu, K. H., and Bitz, C. M.: Chinese  
19 stalagmite  $\delta^{18}\text{O}$  controlled by changes in the Indian monsoon during a simulated  
20 Heinrich event, *Nat. Geosci.*, 4, 474–480, 2011.

21 Peterse, F., Prins, M. A., Beets, C. J., Troelstra, S. R., Zheng, H., Gu, Z., Schouten, S.,  
22 and Damsté, J. S. S.: Decoupled warming and monsoon precipitation in East Asia  
23 over the last deglaciation, *Earth Planet. Sc. Lett.*, 301, 256–264, 2011.

24 Porter, S. C. and An, Z.: Correlation between climate events in the North Atlantic and  
25 China during the last glaciation, *Nature*, 375, 305–308, 1995.

26 Rodwell, M. J., Rowell, D. P., and Folland, C. K.: Oceanic forcing of the wintertime  
27 North Atlantic Oscillation and European climate, *Nature*, 398, 320–323, 1999.

- 1 Schulz, M. and Mudelsee, M.: REDFIT: estimating red-noise spectra directly from  
2 unevenly spaced paleoclimatic time series, *Comput. Geosci.*, 28, 421–426, 2002.
- 3 Schulz, M. and Stattegger, K.: Spectrum: spectral analysis of unevenly spaced  
4 palaeoclimatic time series, *Comput. Geosci.*, 23, 929-945, 1997.
- 5 Shi, Z., Liu, X., Sun, Y., An, Z., Liu, Z., and Kutzbach, J.: Distinct responses of East  
6 Asian summer and winter monsoons to astronomical forcing, *Clim. Past*, 7,  
7 1363–1370, 2011.
- 8 Sun, Y., Clemens, S. C., An, Z., and Yu, Z.: Astronomical timescale and  
9 palaeoclimatic implication of stacked 3.6-Myr monsoon records from the Chinese  
10 Loess Plateau, *Quaternary Sci. Rev.*, 25, 33–48, 2006.
- 11 Sun, Y., Clemens, S. C., Morrill, C., Lin, X., Wang, X., and An, Z.: Influence of  
12 Atlantic meridional overturning circulation on the East Asian winter monsoon, *Nat.*  
13 *Geosci.*, 5, 46–49, 2012.
- 14 Sun, Y., Kutzbach, J., An, Z., Clemens, S., Liu, Z., Liu, W., Liu, X., Shi, Z., Zheng,  
15 W., Liang, L., Yan, Y., and Li, Y.: Astronomical and glacial forcing of East Asian  
16 summer monsoon variability, *Quaternary Sci. Rev.*, 115, 132-142, 2015.
- 17 Sun, Y., Wang, X., Liu, Q., and Clemens, S. C.: Impacts of post-depositional  
18 processes on rapid monsoon signals recorded by the last glacial loess deposits of  
19 northern China, *Earth Planet. Sc. Lett.*, 289, 171–179, 2010.
- 20 Vautard, R., Yiou, P., and Ghil, M.: Singular-spectrum analysis: a toolkit for short,  
21 noisy chaotic signals, *Physica D: Nonlinear Phenomena*, 58, 95-126, 1992.
- 22 Wang, L., Sarnthein, M., Erlenkeuser, H., Grimalt, J., Grootes, P., Heilig, S., Ivanova,  
23 E., Kienast, M., Pelejero, C., Pflaumann, U.: East Asian monsoon climate during the  
24 Late Pleistocene: high-resolution sediment records from the South China Sea, *Mar.*  
25 *Geol.*, 156, 245–284, 1999.
- 26 Wang, P., Clemens, S., Beaufort, L., Braconnot, P., Ganssen, G., Jian, Z., Kershaw, P.,  
27 Sarnthein, M.: Evolution and variability of the Asian monsoon system: state of the art

1 and outstanding issues, *Quaternary Sci. Rev.*, 24, 595-629, 2005.

2 Wang, Y., Cheng, H., Edwards, R. L., An, Z., Wu, J., Shen, C., and Dorale, J. A.: A  
3 high resolution absolute-dated late Pleistocene monsoon record from Hulu Cave,  
4 China, *Science*, 294, 2345–2348, 2001.

5 Wang, Y., Cheng, H., Edwards, R.L., Kong, X., Shao, X., Chen, S., Wu, J., Jiang, X.,  
6 Wang, X., and An, Z.: Millennial and orbital-scale changes in the East Asian  
7 monsoon over the past 224,000 years, *Nature*, 451, 1090–1093, 2008.

8 Xiao, J., Porter, S. C., An, Z., Kumai, H., and Yoshikawa, S.: Grain size of quartz as  
9 an indicator of winter monsoon strength on the Loess Plateau of central China during  
10 the last 130,000 yr, *Quaternary Res.*, 43, 22–29, 1995.

11 Yang, S. and Ding, Z.: A 249 kyr stack of eight loess grain size records from northern  
12 China documenting millennial-scale climate variability, *Geochem. Geophys. Geosy.*,  
13 15, 798–814, 2014.

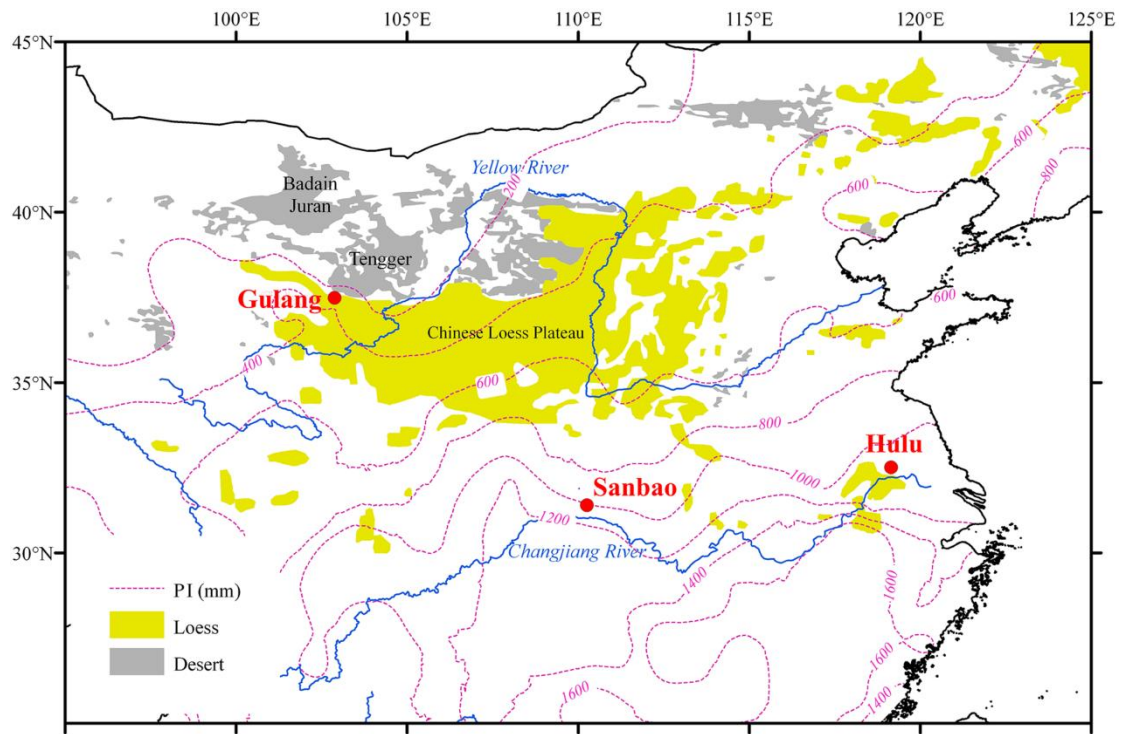
14 Yang, Z., Lin, Z., and Yu, M.: Multi-scale analysis of East Asian winter monsoon  
15 evolution and Asian inland drying force (in Chinese), *Quaternary Sci.*, 31, 73–80,  
16 2011.

17 Yang, Z., Lin, Z., Yu, M., Zhang, Z.: Significant multi-scale analysis on evolution of  
18 the East Asian summer monsoon on the Loess Plateau during the last 1 MaB.P. (in  
19 Chinese), *Geography and Geo-information Science*, 24, 93-97, 2008.

20 Yuan, D., Cheng, H., Edwards, R. L., Dykoski, C. A., Kelly, M. J., Zhang, M., Qing,  
21 J., Lin, Y., Wang, Y., Wu, J., Dorale, J. A., An, Z., and Cai, Y.: Timing, duration, and  
22 transitions of the last interglacial Asian monsoon, *Science*, 304, 575–578, 2004.

23 Zhang, R. and Delworth, T. L.: Simulated tropical response to a substantial  
24 weakening of the Atlantic thermohaline circulation, *J. Climate*, 18, 1853–1860, 2005.

25

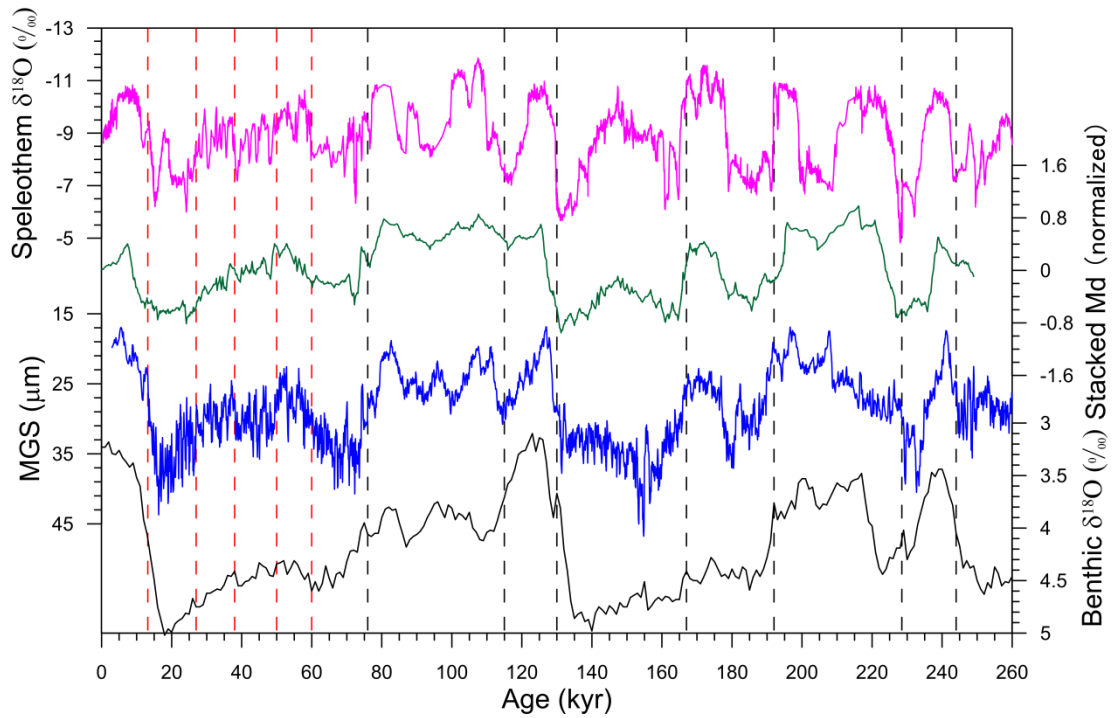


1

2 Figure 1. Map showing the loess distribution and locations of Gulang loess section,

3 Sanbao, and Hulu caves. Dotted lines indicate the precipitation isohyets (PI).

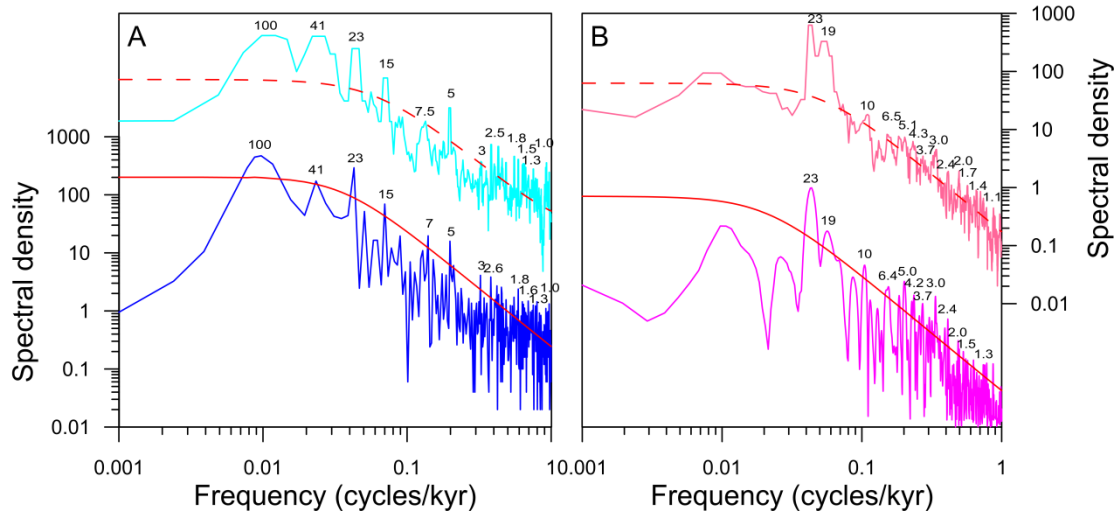
4



1

2 Figure 2. Comparison of Gulang MGS (blue) and CHILOMOS stack Median grain  
 3 size (Md, green, [Yang and Ding, 2014](#)) with the benthic  $\delta^{18}\text{O}$  (black, [Isiecki and](#)  
 4 [Raymo, 2005](#)) and Sanbao/Hulu speleothem  $\delta^{18}\text{O}$  (magenta, [Wang et al., 2008](#); [Cheng](#)  
 5 [et al., 2009](#)) records. The red and black dashed lines denote tie points derived from  
 6 OSL dating and benthic  $\delta^{18}\text{O}$  correlation, respectively.

7

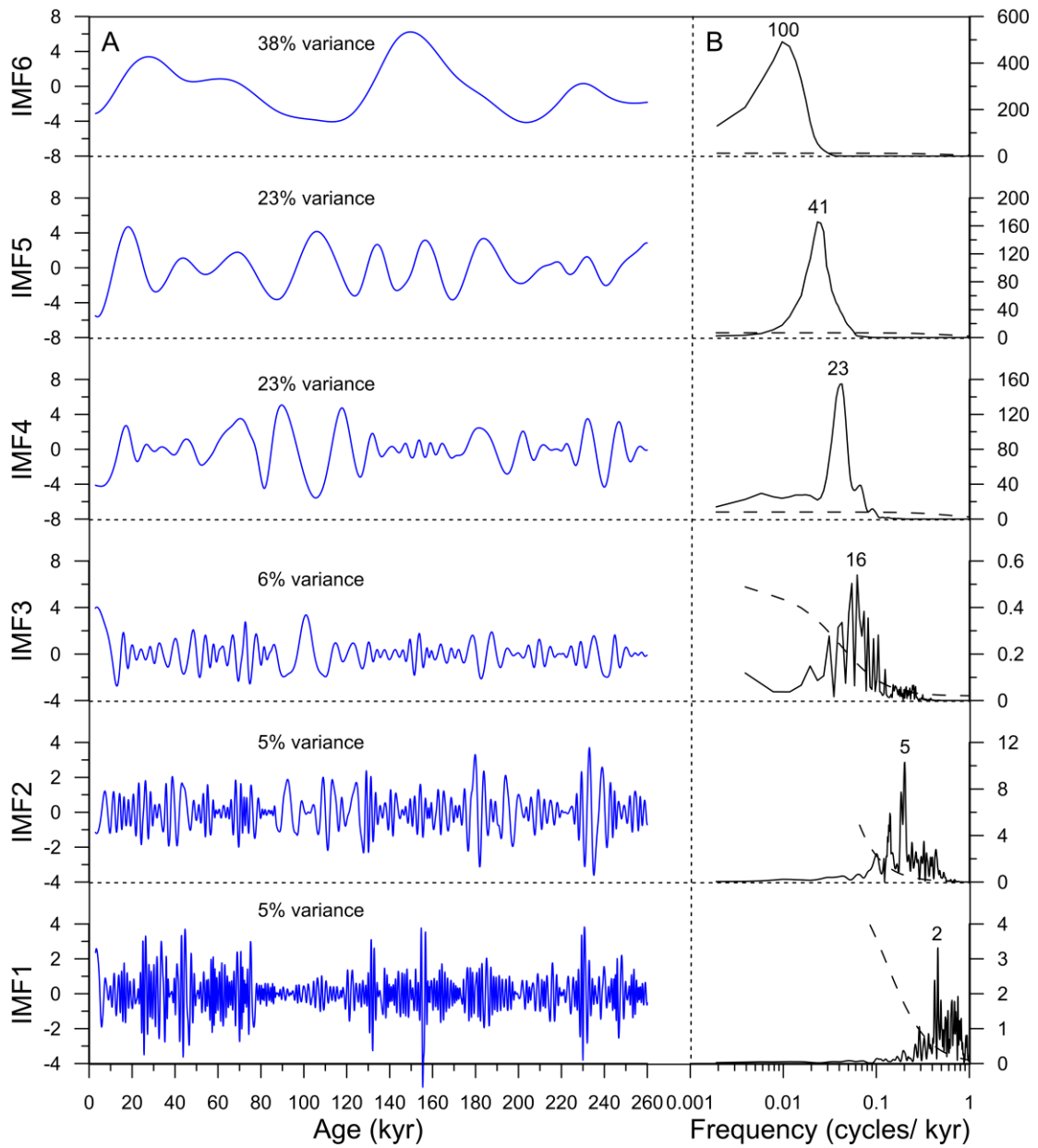


1

2 Figure 3. Spectrum results of Gulang MGS (A) and Sanbao/Hulu speleothem  $\delta^{18}\text{O}$  (B)  
 3 (Wang et al., 2008; Cheng et al., 2009) records using REDFIT (lower) and MTM  
 4 (higher) methods. The red lines represent the 80% (solid) and 90% (dotted)  
 5 confidence levels. Periodicities are shown above the spectral curves.

6



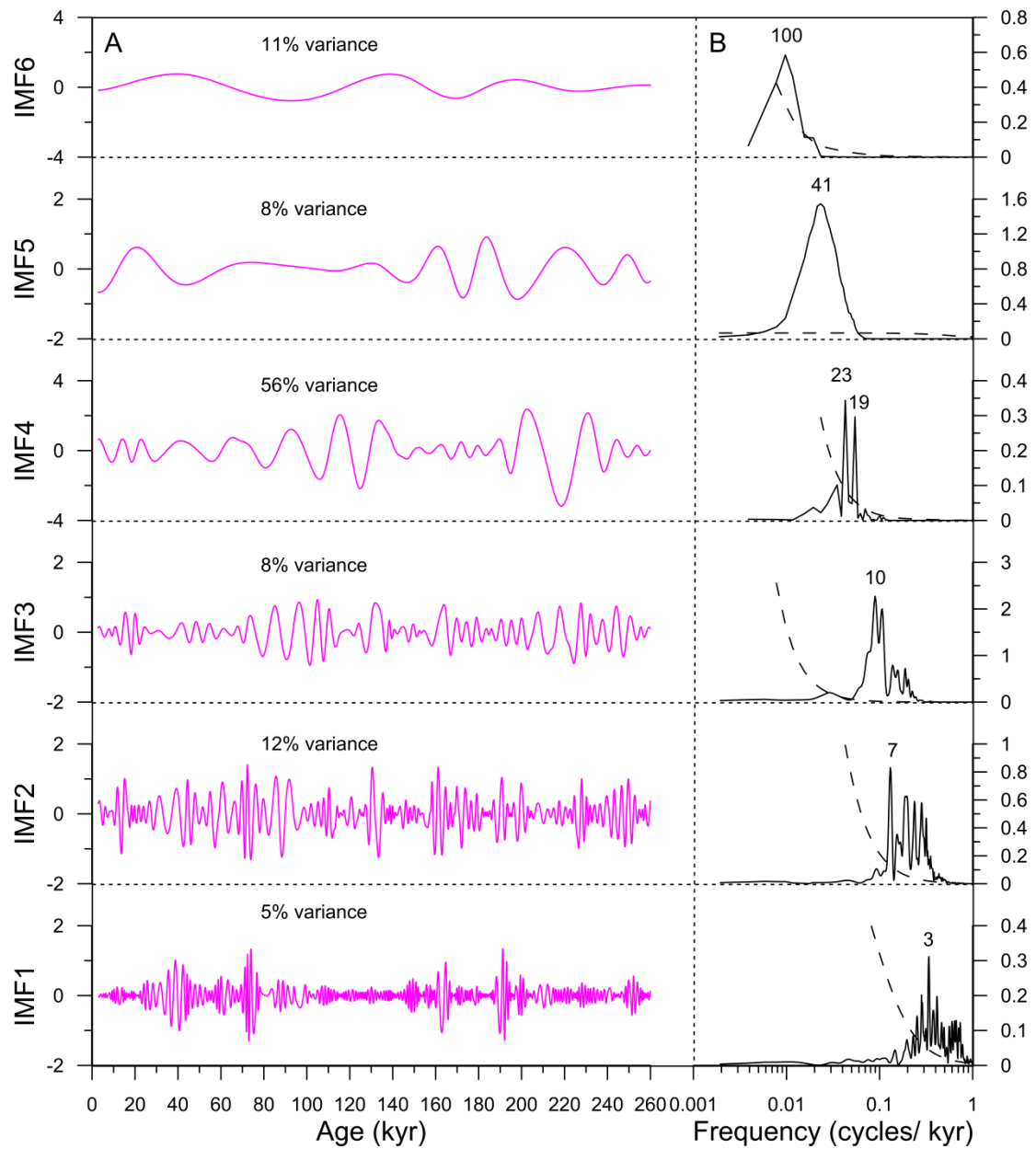


1

2 Figure 4. IMFs of Gulang MGS series (A) and corresponding spectrum (B). Black

3 numbers are dominant periods and dotted lines represent the 90% confidence level.

4

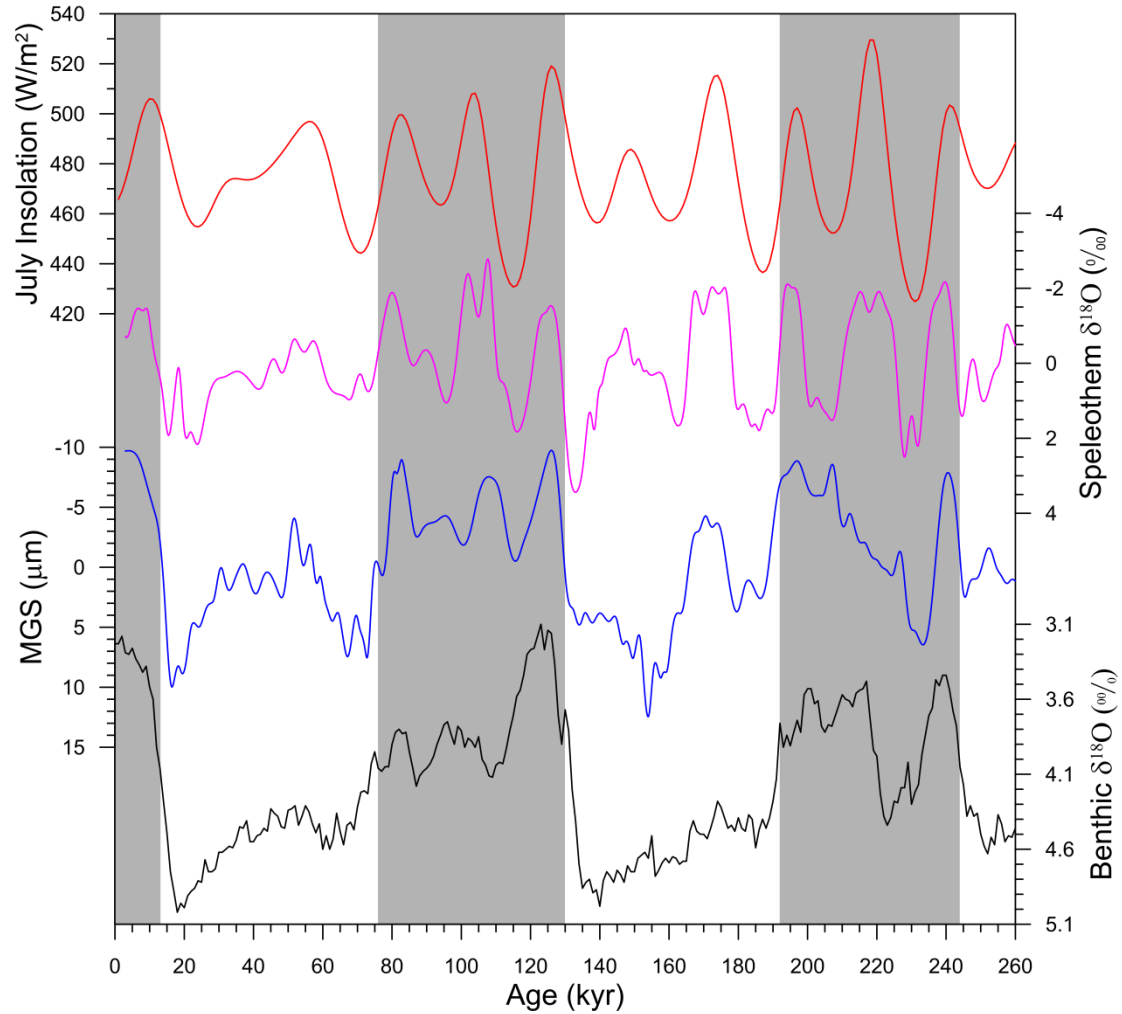


1

2 Figure 5. IMFs of speleothem  $\delta^{18}\text{O}$  series (A) and corresponding spectrum (B). Black

3 numbers are dominant periods and dotted lines represent the 90% confidence level.

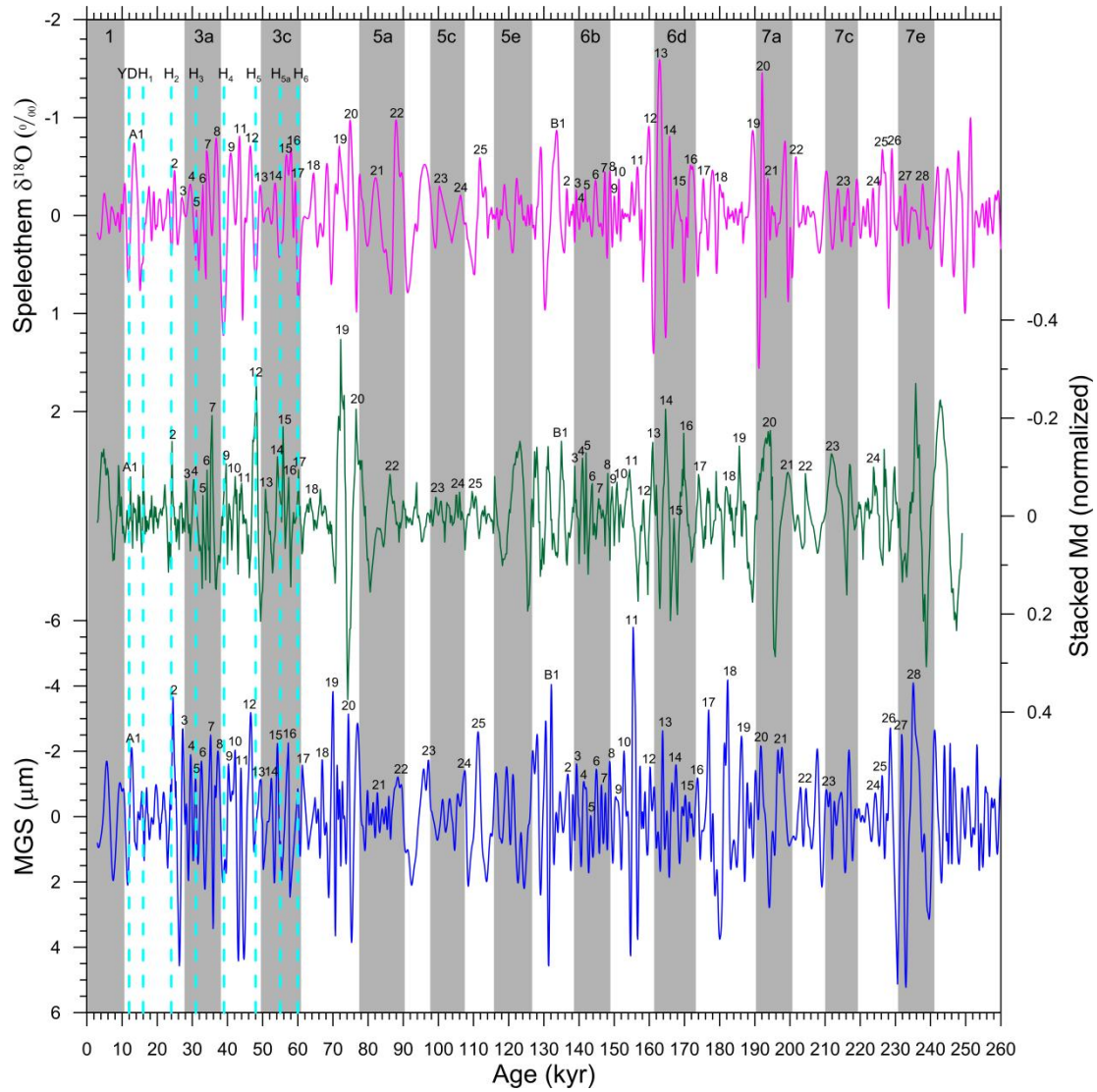
4



1

2 Figure 6. Comparison of the glacial-and-orbital scale components of Gulang MGS  
 3 (blue) and Sanbao/Hulu speleothem  $\delta^{18}\text{O}$  (magenta, Wang et al., 2008; Cheng et al.,  
 4 2009) records with summer insolation at 65 N (red, Berger, 1978) and benthic  $\delta^{18}\text{O}$   
 5 record (black, Lisiecki and Raymo, 2005). The vertical gray bars represent the  
 6 interglacial periods.

7



1

2 Figure 7. Comparison of millennial-scale variations among Gulang MGS (blue),  
 3 CHILOMOS stack Md (green, [Yang and Ding, 2014](#)) and Sanbao/Hulu speleothem  
 4  $\delta^{18}\text{O}$  (magenta, [Wang et al., 2008](#); [Cheng et al., 2009](#)) records over the last two  
 5 glacial-interglacial cycles. Cyan dotted lines are the YD and the Heinrich events  
 6 recorded in the three records and gray bars indicate interglacial periods. The numbers  
 7 represent well-correlated Chinese interstadials identified among the three records.

8